Scenario of the 1996 volcanic tsunamis in Karymskoye Lake, Kamchatka, inferred from X-ray tomography of heavy minerals in tsunami deposits

Simon Falvard[a], Raphaël Paris[a,*], Marina Belousova[b], Alexander Belousov[b], Thomas Giachetti[c], Stéphanie Cuven[d]

[a] Université Clermont Auvergne, CNRS, IRD, OPGC, Laboratoire Magmas et Volcans, F-63000 Clermont-Ferrand, France
[b] Institute of Volcanology and Seismology, Petropavlosk-Kamchatsky, Russia
[c] Department of Earth Sciences, University of Oregon, Eugene, USA.
[d] IODP-France, 14 Av. Edouard Belin, 31400 Toulouse, France.

ARTICLE INFO

ABSTRACT

The concentration and distribution of heavy minerals in tsunami deposits is not random and mostly source-dependent. Heavy minerals may thus be good indicators of sediment provenance and tsunami flow dynamics. The tsunamis generated by the 1996 phreato-magmatic eruption in Karymskoye Lake represent a relevant case-study because the provenance of the abundant heavy minerals found in the tsunami deposits is well constrained (the on-going basaltic eruption itself). X-ray computed tomography (X-CT) of cores of tsunami sediments is used to identify heavy minerals and characterise their source and spatial distribution in the tsunami deposit, and to propose a scenario of the coupled eruption and tsunamis. An original combination of methods including X-CT, SEM and XRF core scanner allows distinguishing subunits corresponding to pulses of sediments deposition and associated inputs of heavy minerals, together with erosive contacts, laminations, and rip-up clasts of the substratum. The structure of the tsunami deposits suggests that a major tsunami consisting of two main waves inundated the coastal terrace up to 100 m inland on the eastern shore of the lake; a scenario that is consistent with waves generated by experimental explosions. This largest tsunami might have occurred when underwater explosions were at a critical water depth of 40 m (corresponding to a two-third submerged explosion in the 60 m deep lake). However, more investigations are needed to better understand the critical conditions leading to a tsunami during underwater eruptions.

1. Introduction

Heavy minerals in clastic sediments and sedimentary rocks are commonly used to study diagenesis, weathering processes, sediment provenance, depositional processes, and to reconstruct paleoenvironments (e.g. Dill, 1998; Mange and Wright, 2007). Heavy minerals are often reported in tsunami deposits (e.g. Switzer et al., 2005, 2012; Bahlburg and Weiss, 2006; Szczuciński et al., 2006; Babu et al., 2007; Morton et al., 2007, 2008; Narayana et al., 2007; Higman et al., 2008; Srinivasalu et al., 2008; Jagodziński et al., 2009, 2012; Moore et al., 2011; Costa et al., 2015). A higher concentration of heavy minerals was estimated in tsunami deposits (Jagodziński et al., 2009) and post-tsunami deposits (Babu et al., 2007) sediments, compared to pre-tsunami deposits. Heavy minerals described in recent tsunami deposits are likely concentrated in pockets or laminae (e.g. Morton et al., 2007; Higman et al., 2008; Srinivasalu et al., 2008; Jagodziński et al., 2012; Switzer et al., 2012). Jagodziński et al. (2009) noted that higher mica

concentrations occurred towards the upper part of the 2004 tsunami deposits in Thailand, with mica flakes found more commonly in the finest-grained sediment samples. However, the 2011 Tohoku-oki tsunami deposits in Sendai, which are particularly rich in heavy minerals, show no different assemblage compared to other pre-tsunami sediments and no vertical trends with a 1 cm-interval sampling (Jagodziński et al., 2012). Predominance of local sediments (beach, dune, soil) upon offshore sediments is confirmed by the rarity of marine bioclasts in the 2011 tsunami deposits at Sendai (Pilarczyk et al., 2012; Szczuciński et al., 2012).

The concentration and distribution of heavy minerals in tsunami deposits is mostly source-dependent, but they are promising indicators of sediment provenance and flow dynamics. Cuven et al. (2013) concluded that "further investigations are needed to improve understanding of the spatial distribution of different populations of grains, in terms of density and shape, and their relationship to sediment sorting in tsunami deposits". In this new contribution, X-ray tomography is used

---

to (1) identify heavy minerals and characterise their source and spatial distribution in a tsunami deposit, and (2) to propose a scenario of the 1996 volcanic tsunamis in Karymskoye Lake (Kamchatka, Eastern Siberia, Russia). This tsunami is a good candidate because the heavy mineral population is mostly provided by the sublacustrine volcanic eruption that generated the tsunami. The approach might give some insights on the coupling between the eruption and the tsunami(s) and understanding of wave generation during phreatomagmatic eruptions. Volcanic tsunamis are generated by a variety of mechanisms, including volcano-tectonic earthquakes, slope instabilities on volcano flanks, pyroclastic flows, underwater explosions, shock waves, and caldera collapse (e.g. Paris, 2015). Among the historical record, volcanic tsunamis represent a low-frequency hazard (about 5% of all recorded tsunamis) but four events (Ritter Island 1888, Krakatau 1883, Unzen 1792, and Oshima-Oshima 1741) are ranked in the twenty deadliest volcanic disasters (Auker et al., 2013).

2. The 1996 eruption and tsunamis in Karymskoye Lake

Karymskoye Lake fills the late Pleistocene Akademii Nauk caldera, the later belonging to the Eastern Volcanic Belt of Kamchatka Peninsula. The lake is 4 km across, with steep flanks and a flat bottom at 60–65 m deep (Fig. 1). This ~0.5 km³ volume of fresh water is fed by several streams and hot springs, and drained by the Karymskaya River to the North (Belousov and Belousova, 2001). The post-caldera volcanic history is poorly documented and apparently limited to scoria cones and tuff rings on the northern shores of the lake (Belousov et al., 1997). Eruptive vents are aligned along a North-South fault linking the

Akademii Nauk caldera to Karymsky stratovolcano, one of the most active volcanoes in Kamchatka.

After a strong earthquake on January 1st, 1996, there was an intense seismic swarm and two eruptions started simultaneously from Karymskoye Lake and from the central vent of Karymsky volcano on January 2nd (Muravyev et al., 1998). Phreatomagmatic activity formed a new tuff-ring attached to the northern slope of the lake. The ice covering the lake might have prevented the generation of tsunami waves during the first stages of the eruption. Pyroclastic base surges damaged bushes as far as 1.3 km from the vent in all directions, at elevations up to 150 m above the level of the lake (Belousov and Belousova, 2001). Ash fall deposits extend mostly to the southeast, with a thickness decreasing from 5 cm at 1.5 km from the vent to 1 cm at > 3 km from the vent on the shores of the lake. Large ballistic blocks of juvenile basalt, hydrothermally altered rocks and rhyodacitic pumice were ejected (Grib, 1998; Belousov and Belousova, 2001). Observation of empty bomb sags in September 1996 was interpreted as an evidence of ice blocks ejected during initial explosions (Belousov and Belousova, 2001).

Tsunamis generated by underwater explosions were observed during helicopter flight and periodically triggered debris flows in the Karymskaya River (Muravyev et al., 1998). Belousov and Belousova (2001) described the effects of the tsunamis on the shores of the lake, and Belousov et al. (2000) estimated wave runups. The values of runup decrease with the distance from the source, i.e. the eruptive vent, with a maximum runup of 19 m on the north-western shore (< 1 km from the vent) and a minimum runup of 1.8 m on the south-eastern shore (3 km from the vent). Boulders of volcanic tuff up to 1.3 m³ were transported
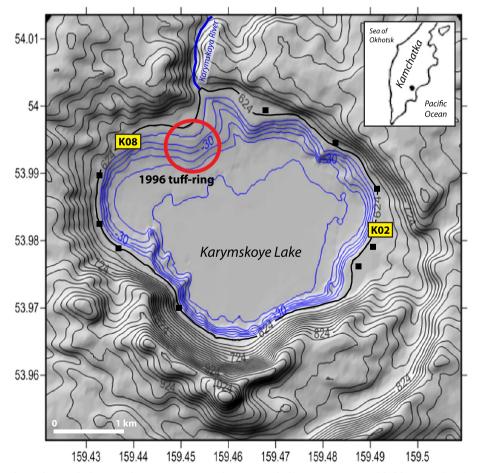

Fig. 1. Location map of Karymskoye Lake, Kamchatka Peninsula, Russia. Reconstructed pre-eruption bathymetric contours (modified from Torsvik et al., 2010) are in meters below the surface of the lake (black bold line at 624 m a.s.l.). Red circle indicates the location of the tuff-ring formed during the 1996 eruption. Deposits of the 1996 tsunami were studied all around the lake (black squares), and the sections sampled for X-ray tomography are indicated by yellow squares (K02 and K08). Geographical coordinates in decimal degrees. (For interpretation of the references to color in this figure legend, the reader is referred to the web version of this article.)
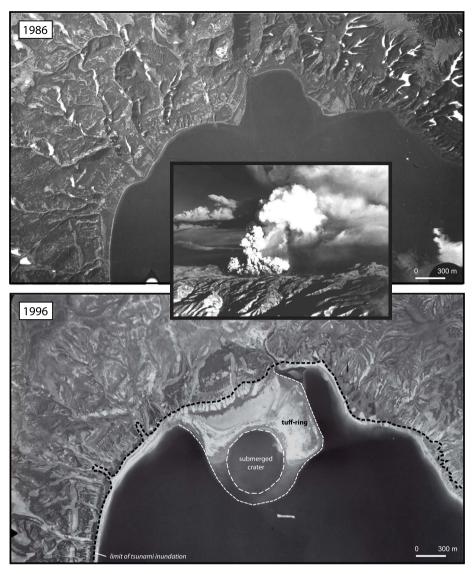
Fig. 2. Effects of the 1996 eruption and tsunamis on the northern shore of Lake Karymskoye. Note the formation of a new tuff-ring with an inner diameter of 500 m, extensive destruction of the vegetation (bush) and erosion of the shoreline, formation of new beaches, and slope erosion near the eruptive vent. Modified from Paris (2015). Photograph showing the volcanic ash plume generated by one of the phreatomagmatic explosions (courtesy of Ya. D. Muravyev).

up to 60 m inland. Soil erosion by successive tsunamis led to the formation of talus up to 2–3 m high all around the lake, except on the southern rocky shore. Sediment reworked by tsunami waves left new beaches up to 50 m wide and sandy patches on terraces behind the talus (Fig. 2). These tsunami deposits are often > 1 m thick on the beach, but < 30 cm on the terraces and gentle slopes, and display a complex inner structure. The mean grain size of the tsunami deposits (from fine to coarse sands) is similar to distal base surge and fallout deposits produced by the volcanic eruption, but tsunami deposits have a wider range of sorting values (Belousov and Belousova, 2001). Deposits forming the emerged part of the tuff-ring are significantly less sorted and coarser-grained (coarse sand to pebble) than the other deposits. The limit of inundation can be traced by drift wood and rounded pumice lapilli (coming from old rhyolitic pyroclastic deposits of the caldera).

Belousov and Belousova (2001) argued that a large tsunami (larger than the ones observed from helicopter) occurred at the end of the eruption, mostly because the tsunami deposits and areas eroded by tsunami waves are not covered by pyroclastic fall deposits. The wave runups measured all around the lake would then correspond to this tsunami. Numerical simulations of underwater explosions and related tsunamis in the lake (Ulvrová et al., 2014) demonstrated that an

underwater explosion of 5×10^{14} J generating a water cavity with a diameter of 350 m and an initial surface displacement of 55 m can explain the observed runups of the largest tsunami.

3. Methods

Survey on the shores of Karymskoye Lake (Kamchatka, Russia) was carried out in August 2009. Tsunami deposits were retrieved in plastic boxes (blocks) and carbon tubes (cores), thus preserving their structure (Fig. 3). Bulk samples were collected along trenches for grain size analysis (laser diffraction on H_2O_2 treated sediment) and composition (binocular). Thin-sections were made for each box sample using dehydration by water-acetone-epoxy-exchange, and analysed with a SEM (JEOL JSM-5910, Laboratoire Magmas & Volcans, Clermont-Ferrand, France). Chemical analyses were performed on dehydrated blocks of sediments using an Avaatech X-ray Fluorescence (XRF) core scanner (EPOC laboratory, Bordeaux). High-resolution chemical relative element variations were captured at the surface of the sediment every 500 µm with a ionization energy of 10 kv.

X-ray Computed Tomography (X-CT) of the tsunami sediments in carbon tubes was realised using (1) an Explore CT-120 GE Healthcare (INSERM Clermont-Ferrand) at a resolution of 50 µm per voxel, and (2)

Fig. 3. Example of sampling at site K02-9 (eastern shore of the lake). Bulk sampling (white dots) of the 1996 tsunami deposit (K02-9A to K02-9D) and pre-tsunami sediments (K02-9E). The tsunami deposit is also sampled using carbon tubes (cores for X-ray tomography) and plastic boxes (for thin sections). Note the 20 cm-large rip-up clast of white ash at the base of the tsunami deposit (on the left).

the ESRF beamline ID19 (Grenoble, France) at a resolution of 15 μm per voxel (one sample only: K02-9). X-CT is an analytical technique based on the absorption of X-rays by the sample (Hounsfield, 1962). This means that particles of different densities will appear in different shades of grey on the images. Due to their high density, heavy minerals appear in very bright grey to white tones on the X-CT images, which allowed to easily separate them from the other particles by using a simple threshold value. Particles with grey values corresponding to the heavy minerals were turned white and particles and matrix of lower density were turned black. The choice of the threshold value was validated by determination of the minerals on thin sections (mostly olivines, clinopyroxenes and Fe-Ti oxides). The position of each heavy mineral in the core was then automatically measured and saved along 2D vertical slices of the cores. Heavy minerals abundances along the cores were calculated using a 1 mm subsampling step with a Matlab code (see Falvard and Paris, 2016, for more details). The higher resolution of the scans performed at ESRF ID19 (15 μm per voxel) allowed measuring the intermediate diameter (B-axis) of each particle along a vertical slice of the sample, plotting a map of the grain size distribution and measuring GSD (Grain Size Distribution) parameters (using Matlab codes proposed by Falvard and Paris, 2016).

For this study, we focus on 9 trenches along a 25 m long transect on the eastern shore of the lake (K02 on Fig. 1). Belousov et al. (2000) measured runups between 1.8 and 2.4 m on the eastern shore of the lake. Low topography of this area favoured penetration of tsunami waves inland, up to 100 m, even if the wave heights were small compared to the other shores. Transect K02 is oriented N135°, i.e. perpendicular to the shoreline and aligned with the eruptive vent (Fig. 4). The first ten meters of the transect (trenches K02-8 and K02-9) correspond to the new beach formed during the 1996 eruption and tsunamis. The shores of the lake were vegetated by alder bush before the tsunami. Trench K02-7 is on a gentle slope break between the beach and a terrace. The other trenches (K02-1 to K02-6) are located on this terrace that is 1–2 m above the level of the lake (624 m a.s.l.). Roots or

coarse clasts prevented sampling K02-8, K02-5 and K02-6 in carbon tubes. Dehydrated blocks and thin sections were prepared for samples K02-9 (upper 10 cm only) and K02-8. Results obtained on the eastern shore of the lake are compared with a proximal section on the western shore (K08), at 1 km from the source of the tsunamis, i.e. the eruptive vent (Fig. 1).

4. Results

4.1. Characteristics of tsunami deposits on the eastern shore

Preserved thickness of the 1996 tsunami deposits on the eastern shore progressively decreases landward (Fig. 5), from 43 cm on the beach (K02-9) to 3 cm at 30 m from the shoreline (K02-6). This landward thinning is associated with landward fining of the mean grain size, but the tsunami deposits are internally structured in subunits with different characteristics. The contact with the underlying soil and riverbed sediments is always erosive. Rip-up clasts of soil and white compacted ash are frequent (Fig. 3). Thickest section K02-9 displays 4 subunits (A-D). Basal unit (K02-9D) is a massive 23 cm thick dark medium sand with > 50% of fresh (juvenile) basaltic pyroclasts and crystals (plagioclases, olivines and clinopyroxenes) from the 1996 eruption. There is no other possible source of such an assemblage of minerals in the local stratigraphy. Most frequent texture of juvenile basaltic clasts found in the K02 sections is blocky and poorly vesiculated. Texture of the basaltic clasts sampled in the tuff ring ranges from poorly to highly vesiculated, with occasional veins of rhyolite (Grib, 1998; Belousov and Belousova, 2001). The presence of rip-up clasts of soil at the base of the subunit and crude laminations observed on X-CT imagery excludes primary fallout deposition. Subunit KO2-9D has high concentrations of heavy minerals, with two pulses at > 1500 heavy minerals per mm (Fig. 5).

Second subunit 9C scours subunit 9D and a 20 cm-large rip-up clast of white ash marks the contact (Fig. 3). Subunits 9C, 9B, and 9A are all
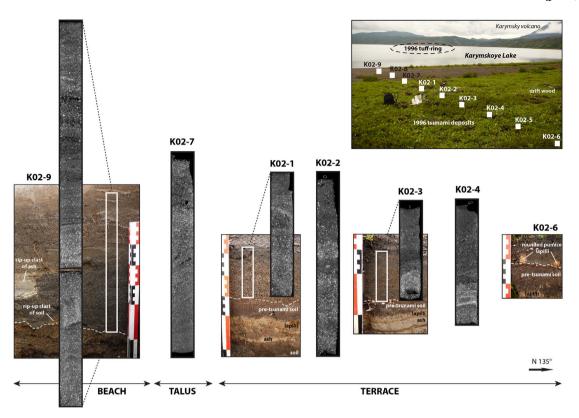
Fig. 4. Longitudinal transect (KO2) in the 1996 tsunami deposit on the eastern shore of Karymskoye Lake. The tsunamis were generated by underwater explosions from the tuff-ring (dotted circle). X-ray tomography was performed on 6 core samples.

laminated: horizontal to weakly oblique laminae of coarse silt to fine sand in 9C, crudely laminated fine to coarse sand in 9B, and cross-laminae of very fine to medium sand in 9A (Figs. 6 and 7). Similar laminations are observed on section K02-8. Compared to the dark sand of basal subunit 9D, the other subunits have less 1996 juveniles (< 40%) and less heavy minerals (< 700 per mm), but more pumice (> 20%) and rare diatoms in subunit 9A. The distribution of pumice clasts in the tsunami deposits is not homogenous and their size ranges from coarse ash to fine lapilli. Sublayers or lines enriched in pumices (40–90%) coinciding with peaks of Si/Ca were identified on thin sections and X-CT (Fig. 8). The concentration of heavy minerals (X-CT) is not grain-size dependent (Fig. 6) and correlates with peaks of Fe/Al and Ca/Al, which represent respectively higher concentrations of oxides (mostly titanomagnetites) and olivines, and clinopyroxenes.

Despite its small size and smooth morphology, the talus between the beach and the terrace (Fig. 4) affected the depositional processes, as evidenced by the structure and texture of tsunami deposits attached on the slope. There are no longer distinct subunits visible on section K02-7, which is obliquely laminated and inversely graded from very fine sand at the base to medium sand at the top. Inverse grading is coupled with an upward increase of the concentration of heavy minerals (Fig. 5). Lamination is dipping downward, the angle being similar to the topography of the talus.

On the terrace but still close to the talus, section K02-1 is poorly organised and no internal structure or vertical grading could be detected on the field. However, X-CT allows distinguishing two successive pulses of medium-to-coarse sand particularly rich in heavy minerals, separated by a horizontal laminae of very fine sands with less
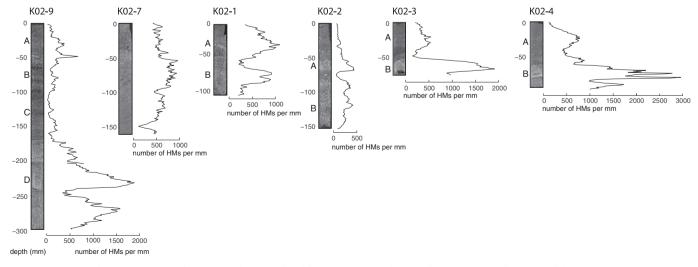

Fig. 5. Concentration of heavy minerals (HMs) inferred from X-CT on cores of tsunami deposits. See Fig. 4 for location of the sections.
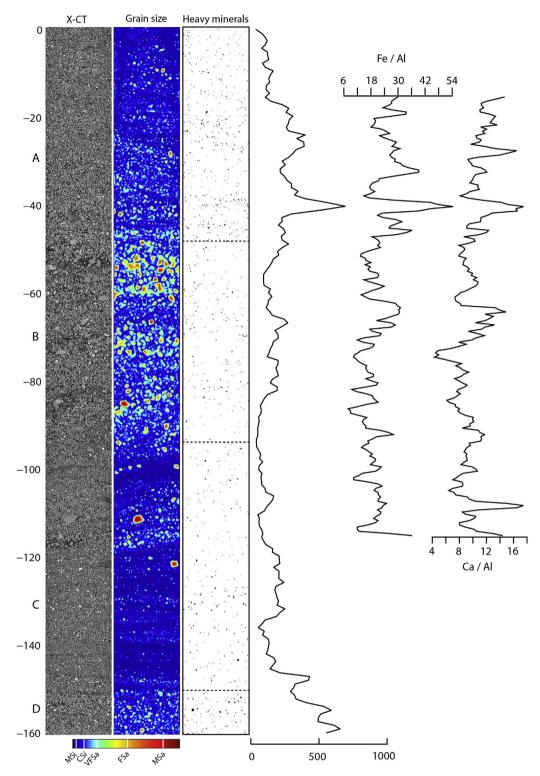
Fig. 6. Concentration of heavy minerals (X-CT, units per mm) compared to grain size inferred from image analysis of X-CT (MSi: medium silt; CSi: coarse silt; VFSa: very fine sand; FSa: fine sand; MSa: medium sand), and major element chemistry (XRF) of the upper part of section K02-9 (subunits A, B and C). The maximum values in Fe/Al and Ca/Al profiles represent respectively higher concentrations of oxides (titanomagnetite) + olivines, and clinopyroxenes.

heavy minerals (at − 50 mm on Fig. 5). Similar structure is found on the following sections (K02-2 to K02-6), with lower concentrations of heavy minerals at K02-2 (< 500 per mm) and higher concentrations at the base of sections K02-3 and K02-4 (> 1500 per mm). High concentrations of heavy minerals are associated with high proportions (> 50% at the binocular) of juvenile material from the 1996 eruption such as basaltic pyroclasts and phenocrysts of plagioclase, olivine, and

clinopyroxene. Similar stratigraphy was found on other trenches located along the eastern shore of the lake (Fig. 1). In this area, terraces higher than 2 m systematically prevented the deposition of sediments by tsunami waves further inland. Note that the upper limit of tsunami deposits coincides with the upper limit of driftwood. Thus, the absence of tsunami deposits does not mean that they were not preserved at elevations higher than 2 m above the level of the lake.
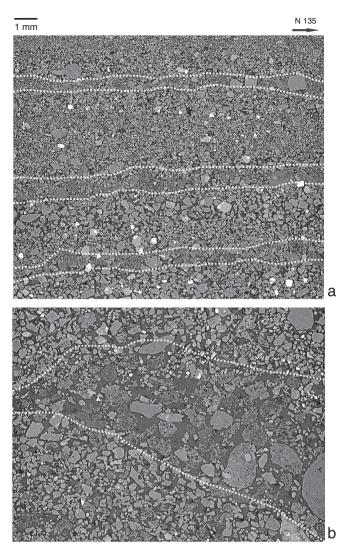
Fig. 7. Cropped views of sample K02-9 scanned at ESRF ID19. The resolution is 15 μm/voxel. Heavy minerals are in bright white and thus easy to identify throughout the deposit. a — Subhorizontal lamination in the intermediate part of the deposit (subunit K02-9C). Almost invisible to the naked eye, laminations appear clearly on the X-ray imagery due to the low density of pumices intercalated between sand grains. Note the fine-scale vertical grading in each laminae. b — Landward plunging stratification in the upper part of the deposit (subunit A), mostly composed of coarse pumices (notice the vesiculation inside the pumice clasts) and large volumes of porosity between layers of finer sands and silts.

4.2. Characteristics of tsunami deposits on the western shore

High terraces or steep slopes of the western side (K08) also limited inundation and deposition to the beach, where the 1996 tsunami deposits are particularly thick (commonly > 50 cm). Belousov et al. (2000) reported wave runups higher than 5 m in this area. Due to a different topographic setting and closer distance to the source, the structure of the 1996 tsunami sequence is different. Section K08 displays a complex succession of laminated sands and silts characterised by abrupt variations of grain size (Fig. 9). The base of the tsunami deposit is unclear and > 7 subunits can be distinguished. Low-resolution X-CT on a dehydrated block allows identifying cross-laminae in the upper part of the sequence (subunit K08-B on Fig. 8). This cross-bedding is not associated to any particular distribution of heavy minerals (Fig. 10). The deposits sampled along the western shore of the lake (e.g. K08) are particularly rich in diatoms. The distribution of diatoms is not random, and fine-grained sub-layers or lines enriched in diatoms can be seen intercalated between coarser subunits (Fig. 11).

Although being located at 1 km from the eruptive vent and near the limit of pyroclastic surges, 1996 tsunami deposits of the western shore have always < 30% of juvenile clasts from the 1996 eruption.

5. Discussion

5.1. Distribution of heavy minerals in the tsunami deposits

X-CT proved to be a useful technique to detect heavy minerals in the tsunami deposits, with measured abundances ranging from several dozens to 3000 units per millimetre in the samples (Fig. 5), and despite a limited resolution (50 μm for INSERM scans). Note that 2D analysis could have been done using a mosaic of SEM (Scanning Electron Microscope) images, but X-CT allows working on selected horizontal or vertical slices representing the entire core or specific areas of interest. Comparing grain size data and heavy mineral abundances in the upper part of K02-9 (Fig. 6) shows that the distribution of heavy minerals along the deposit is not random and not grain size dependent. Subunits enriched in heavy minerals are clearly evidenced by the X-CT data. These remarks are also valid for the pumice clasts (Fig. 8), whose behaviour in water waves is probably different from heavy minerals (except micas in a certain extent due to their flaky shapes, but none were found in these deposits). However, heavy minerals in the 1996 tsunami deposits are never distributed along thin laminae, as often described in other tsunami deposits (e.g. Morton et al., 2007; Higman et al., 2008; Srinivasalu et al., 2008; Jagodziński et al., 2012; Switzer et al., 2012). The formation of heavy minerals laminae requires certain sediment concentration and flow regime conditions (e.g. Cheel, 1990) that were apparently not fulfilled during the 1996 Karymskoye Lake tsunami.

Distribution of heavy minerals together with the structure and texture of the tsunami deposits of the lower sections (e.g. K02-9 and K08), confirm that multiple tsunamis were produced during the volcanic eruption. This succession of tsunamis is evidenced by multi-bedded deposits (Fig. 9) whose distribution is limited to the beach (< 1.5 m above the level of the lake). Orientation of the laminations in the upper part of section K02-9 (Figs. 6 and 7) indicates transitions from upper plane beds (horizontal lamination) to low-angle beds dipping landward (dune-like bedforms). Capping subunits are often cross-bedded (Figs. 6 and 10), with either backset orientation if we consider that they were deposited by an uprush flow of the upper regime, or foreset orientation if they correspond to a final backwash or drainout of the lake. In any case, there is no clear relation between the abundance of heavy minerals, the vertical grading and the laminations (Figs. 6 and 10).

However, X-CT reveals two peaks of heavy minerals in subunit K02-9D (Fig. 5), as well as in all sections located on the terrace of the eastern shore (Fig. 5: upper sections K02-1 to K02-4). This transect-scale correlation suggests that two main waves inundated the terrace up to 100 m inland on the eastern shore of the lake. This phase of inundation corresponds to the maximum runup values measured by Belousov et al. (2000). The tsunamis observed during the helicopter flight (Muravyev et al., 1998) did not inundate the terrace of the eastern shore. A larger tsunami, either consisting of two main waves or an uprush-backwash succession, is thus recorded in the distribution of heavy minerals along the upper sections.

5.2. A scenario of the volcanic eruption and tsunamis

It is worth reminding that the explosions were not all tsunamigenic, as they simply produced a single, near-vertical, column-like jet of gas and pyroclasts that collapsed back into the lake, thus generating a subtle base surge. Initial stage of volcanic activity started at a water depth of 45–50 m when the surface of the lake was still covered by a 1 m thick icecap (Fig. 12A). Thus, the first explosions could not generate tsunamis. During a transitional stage (Fig. 12B), the eruption
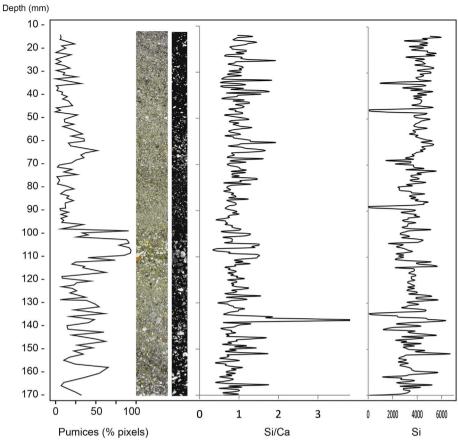
Fig. 8. Distribution of pumices estimated from image analysis of thin sections at the SEM and Si/Ca profile inferred from XRF scan of dehydrated block (sample K02-8).
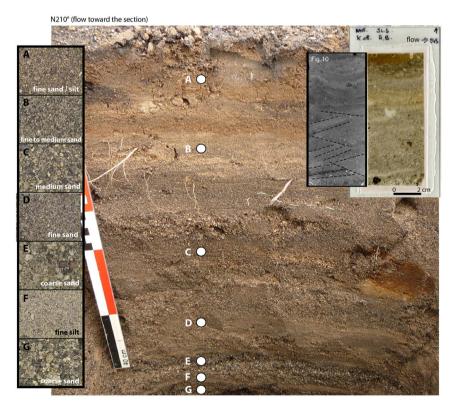

Fig. 9. Overview of section K08 (western shore of the lake). The 1996 tsunami deposit represents the entire thickness trenched and is organised in distinct subunits, which are all laminated (except subunit K08-E and lenses of coarse sand in K08-C). Note the rip-up clasts of soil and ash on the right side and the backset cross-laminae in subunit K08-B (X-CT).
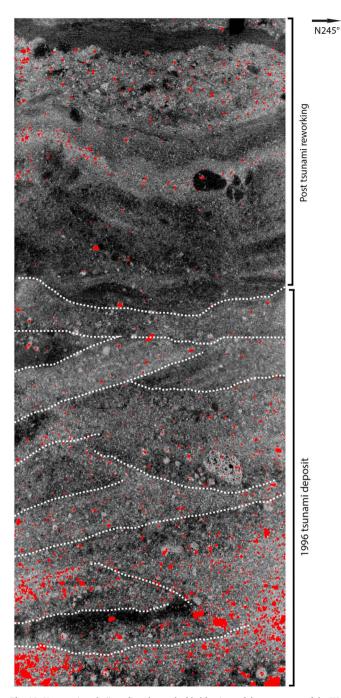
N245°

Post tsunami reworking

1996 tsunami deposit

Fig. 10. Heavy minerals (in red) and cross-bedded laminae of the upper part of the K08 section (see Fig. 9), western shore of the lake.

progressively broke the ice surface and fallout pyroclasts started to accumulate on ice rafts. Water expulsed by the explosions might have surged and redistributed pyroclasts on the surface of the icecap before its complete melting. The first tsunamis then pushed ice rafts covered with pyroclasts on the shores of the lake (Fig. 12C). For areas which were not affected by pyroclastic surges and covered by < 3 cm of ash (e.g. eastern shore), this hypothesis could explain the unexpected high proportion of juvenile basaltic clasts (and heavy minerals) in the thick basal subunits of tsunami deposits (Figs. 3 and 5). Distal pyroclastic surge and fallout deposits settling in the lake between each explosion might have represented an additional source of heavy minerals for the tsunami deposits.

Strongest observed explosions started with a rapidly rising (~3 s), smooth-surfaced bulbous mass of gas and pyroclasts expanding within a

shell of water up to 450 m high (Muravyev et al., 1998; Belousov and Belousova, 2001). This mass then became unstable and was pierced by cypressoid jets of pyroclasts with gas and water. Simultaneously, a bore-like elevation of the water surface started to propagate radially at about 20–40 m·s^{-1} thus forming a tsunami in the lake (Muravyev et al., 1998; Belousov and Belousova, 2001) (Fig. 12D and E). There is no ice anymore on photographs taken by Muravyet et al. (1998) three hours after the beginning of the eruption. This description represents the mature stage of the eruption (Fig. 12E), observed during the helicopter flight. There is no observation available for the initial and final stages. Multiple tsunamis and subsequent reflected waves were generated during the mature stage of the eruption, as evidenced by multi-bedded tsunami deposits of the lower sections (Figs. 3 and 9).

The distribution of heavy minerals in the upper sections (Figs. 4 and 5: terrace along the eastern shore) records two successive waves corresponding to the maximum runup. It is interesting to note that tsunamis generated by underwater explosions consist of two main waves followed by smaller undulations, as demonstrated by experiments and numerical simulations (e.g. Le Méhauté and Wang, 1996; Kedrinskii, 2005; Torsvik et al., 2010; Ulvrová et al., 2014). The water is initially pushed upward and radially, forming a crater and a cylindrical bore expanding radially to form the leading wave, followed by a wave trough. The water crater then collapses as in a dam break model, thus generating a peak of water in the centre and a second cylindrical bore that progressively turns to a non-dissipative wave (Le Méhauté and Wang, 1996). However, a reflected wave or an uprush-backwash succession could also explain the structure and two-peak distribution of heavy minerals. Heavy mineral patches or shadows displaying a downstream decreasing abundance of heavy minerals in the second peak would have supported the backwash hypotheses (Cheel, 1984). However, there are no clear longitudinal trends of increasing or decreasing abundance of heavy minerals along the K02 transect (Fig. 5).

It is actually difficult to state on the origin and precise timing of the largest tsunami (Fig. 12D). The poor quality of the videos taken from the helicopter does not allow identifying traces of erosion on the shores of the lake. Belousov and Belousova (2001) proposed that the largest tsunami occurred at the end of the eruption because its deposits are never covered by ash fallout deposits. Fragments of a hut originally located on the northern shore of the lake (and destroyed by pyroclastic surges and tsunamis) were found in drift wood left by the largest tsunami on the terrace of south-eastern shore. The transport of these debris from one side of the lake to another requires a significant time lapse between the destruction of the hut and the largest tsunami. However, it is difficult to imagine how explosions might have generated large waves when the tuff ring was already well developed and emerging (Fig. 12E). Experimental studies of underwater explosions (e.g. Craig, 1974) demonstrated that maximum wave heights occur for a two-third submerged explosion (i.e. at 40 m water depth in the case of Karymskoye Lake). Wave heights at this upper critical depth are twice that observed for explosions at the lower critical depth (fully submerged, i.e. at 60 m water depth).The eruptive phase corresponding to two-third submerged explosions might have generated the largest tsunami recorded in the stratigraphic sections and distribution of heavy minerals (Fig. 12D).

6. Conclusion

This study confirms that (1) X-CT combined with other methods such as XRF and SEM is a powerful technique for characterising the structure and composition of tsunami deposits (May et al., 2015; Falvard and Paris, 2016), and (2) provides another evidence of volcanic eruption partially reconstructed using its tsunami record (Paris et al., 2014). X-CT helped evidencing the structure and characterising the distribution of heavy minerals in the 1996 tsunami deposits. In this case study, the source of the heavy minerals is controlled by volcanic pulses
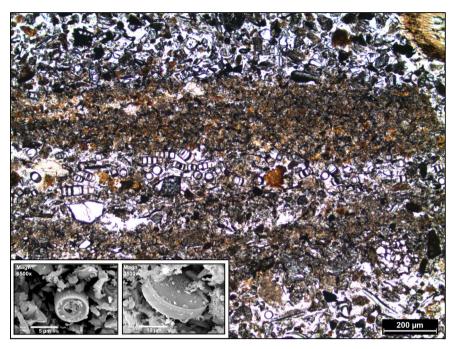
Fig. 11. Diatoms in tsunami sample K08 viewed at the SEM and in thin sections. The distribution of diatoms is not random, and fine-grained sub-layers or lines enriched in diatoms can be seen at the base of coarser subunits.
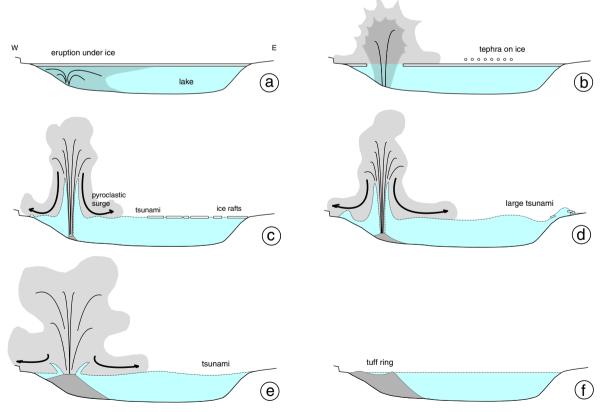

Fig. 12. A scenario of the 1996 volcanic tsunamis in Karymskoye Lake. The lake is 4 km large. Vertical scale exaggerated. a — Initial stage of the phreatomagmatic eruption: a thick ice cap covers the whole surface of the lake, preventing any tsunami to occur; b — Emergent eruption: ice cap is pierced by the explosions, and basaltic pyroclasts (rich in heavy minerals) are scattered on the ice by fallout; c — Transitional stage: melting of the ice allows tsunami waves to propagate in the lake. Ice rafts are pushed towards the shores; d — Mature stage: largest tsunami occurs as an optimal ratio of explosion depth vs. water depth is reached (i.e. two-third submerged explosions); e — Mature stage (as observed during helicopter flight): the growing volcanic edifice gets closer to the surface of the lake and thus hampers the energy transfer from the explosion to the lake, preventing large waves to form; f — Final stage: fully formed tuff ring at the end of the eruption.

(phreatomagmatic explosions) and it was possible to distinguish a large tsunami composed of two main waves corresponding to peaks of heavy mineral abundances.

However, it is still difficult to understand the critical conditions leading to a tsunami during underwater eruptions and to define hazard scenarios for future eruptions of the same style. Magma-water interactions during phreatomagmatic eruptions are complex and their physics is controlled by water depth, geometry of the vent and magma-water interface, transfer of thermal energy, processes of intermingling and mixing between magma and water, metastability of superheated water, and quantity of gas in the ascending magma (Kokelaar, 1986; Wohletz, 1986; Morrissey et al., 2010). Explosive eruptions accompanying the formation of maars and tuff rings, as occurred at Taal in 1965 and Karymskoye in 1996, are characterised by phases of optimal ratios of (a) water vs. magma and (b) explosion (fragmentation) depth vs. water depth. These explosions are able to generate tsunamis, whereas most of the Surtseyan-type explosions are not (Kokelaar, 1986; Paris, 2015).

Underwater eruptions represent < 10% of all recorded eruptions (if we exclude eruptions at mid-ocean ridges) but they caused 20% of all fatalities related to volcanic activity in historical time, including fatalities due to tsunamis (Mastin and Witter, 2000). Hazard of volcanic tsunamis in lakes is particularly concerning and somewhat neglected (Freundt et al., 2007; Paris, 2015) if we consider that the coasts of many volcanic lakes in the world are densely populated (e.g. Lake Nicaragua and Lake Managua in Nicaragua, Lake Kivu in the Democratic Republic of Congo, Lake Taal in the Philippines).

Acknowledgments

References

Auker, M.R., Sparks, R.S.J., Siebert, L., Crosweller, H.S., Ewert, J., 2013. A statistical analysis of the global historical volcanic fatalities record. J. Appl. Volcanol. 2013 (2:2).

Babu, N., Babu, D., Das, P., 2007. Impact of tsunami on texture and mineralogy of a major placer deposit in southwest coast of India. Environ. Geol. 52, 71–80.

Bahlburg, H., Weiss, R., 2006. Sedimentology of the December 26, 2004 Sumatra tsunami deposits in eastern India (Tamil Nadu) and Kenya. Int. J. Earth Sci. 96 (6), 1195–1209.

Belousov, A., Belousova, M., 2001. Eruptive process, effects and deposits of the 1996 and ancient basaltic phreatomagmatic eruptions in Karymskoye lake, Kamchatka, Russia. In: White, J., Riggs, N. (Eds.), Volcaniclastic Sedimentation in Lacustrine Settings. 30. Blackwell, International Association of Sedimentologists Special Publications, pp. 235–260.

Belousov, A., Belousova, M., Muravyev, Y., 1997. Holocene eruptions in Akademiya Nauk caldera and the age of Karymsky stratovolcano, Kamchatka. Transactions of the Russian Academy of Sciences, Earth Sciences Section 335, 653–657.

Belousov, A., Voight, B., Belousova, M., Muravyev, Y., 2000. Tsunamis generated by subaquatic volcanic explosions: unique data from 1996 eruption in Karymskoye lake, Kamchatka, Russia. Pure Appl. Geophys. 157, 1135–1143.

Cheel, R.J., 1984. Heavy mineral shadows, a new sedimentary structure formed under upper flow regime conditions: its directional and hydraulic significance. J. Sediment. Petrol. 54, 1173–1180.

Cheel, R.J., 1990. Horizontal lamination and the sequence of bed phases and stratification under upper-flow-regime conditions. Sedimentology 37, 517–529.

Costa, P.J.M., Andrade, C., Cascalho, J., Dawson, A.G., Freitas, M.C., Paris, R., Dawson, S., 2015. Onshore tsunami sediment transport mechanisms inferred from heavy mineral assemblages. The Holocene 25 (5), 795–809.

Craig, B.G., 1974. Experimental Observations of Underwater Detonations Near the Water Surface. Los Alamos Scientific Laboratory of the University of California (report LA-5548-MS, UC-34).

Cuven, S., Paris, R., Falvard, S., Miot-Noirault, E., Benbakkar, M., Schneider, J.-L., Billy, I., 2013. High-resolution analysis of a tsunami deposit: case-study from the 1755 Lisbon tsunami in southwestern Spain. Mar. Geol. 337, 98–111.

Dill, H.G., 1998. A review of heavy minerals in clastic sediments with case studies from the alluvial-fan through the nearshore-marine environments. Earth Sci. Rev. 45, 103–132.

Falvard, S., Paris, R., 2016. X-ray tomography of tsunami deposits: towards a new depositional model of tsunami deposits. Sedimentology 64 (2), 453–477.

Freundt, A., Strauch, W., Kutterolf, S., Schmincke, H.-U., 2007. Volcanogenic tsunamis in lakes: examples from Nicaragua and general implications. Pure Appl. Geophys. 164, 527–545.

Grib, E.N., 1998. Petrology of ejecta discharged by the January 2–3 eruption in the Akademii Nauk caldera. Vulkanol. Seismol. 5, 71–97.

Higman, B., Bourgeois, J., Shiki, T., 2008. Deposits of the 1992 Nicaragua tsunami. In: Tsuji, Y., Yamazaki, T., Minoura, K. (Eds.), Tsunamiites – Features and Implications. Elsevier, pp. 81–103.

Hounsfield, G.N., 1962. Computerized transverse axial scanning (tomography): part 1. Description of system. Br. J. Radiol. 46 (552), 1016–1022.

Jagodziński, R., Sternal, B., Szczuciński, W., Lorenc, S., 2009. Heavy minerals in 2004 tsunami deposits on Kho Khao Island, Thailand. Pol. J. Environ. Stud. 18, 103–110.

Jagodziński, R., Sternal, B., Szczuciński, W., Chagué-Goff, C., Sugawara, D., 2012. Heavy minerals in the 2011 Tohoku-oki tsunami deposits — insights into sediment sources and hydrodynamics. Sediment. Geol. 282, 57–64.

Heavy minerals in use. In: Mange, M.A., Wright, D.T. (Eds.), Developments in Sedimentology. 58 Elsevier (1283 pp.).

Kedrinskii, V.K., 2005. Hydrodynamics of Explosion. Springer, Berlin, Heidelberg.

Kokelaar, P., 1986. Magma-water interactions in subaqueous and emergent basaltic volcanism. Bull. Volcanol. 48, 275–289.

Le Méhauté, B.L., Wang, S., 1996. Water waves generated by underwater explosion. Adv. Ser. Ocean Eng. World Sci, New Jersey.

Mastin, L.G., Witter, J.B., 2000. The hazards of eruptions through lakes and seawater. J. Volcanol. Geotherm. Res. 97, 195–214.

May, S.M., Falvard, S., Norpoth, M., Pint, A., Brill, D., Engel, M., Scheffers, A., Dierick, M., Paris, R., Squire, P., Brückner, H., 2015. A mid-Holocene candidate tsunami deposit from the NW Cape (Western Australia). Sediment. Geol. 332, 40–50.

Moore, A., Goff, J., McAdoo, B.G., Fritz, H.M., Gusman, A., Kalligeris, N., Kalsum, K., Susanto, A., Suteja, D., Synolakis, C.E., 2011. Sedimentary deposits from the 17 July 2006 Western Java tsunami, Indonesia: use of grain size analyses to assess tsunami flow depth, speed, and traction carpet characteristics. Pure Appl. Geophys. 167 (11), 1951–1961.

Morrissey, M., Gisler, G., Weaver, R., Gittings, M., 2010. Numerical model of crater lake eruptions. Bull. Volcanol. 72, 1169–1178.

Morton, R.A., Gelfenbaum, G., Jaffe, B.E., 2007. Physical criteria for distinguishing sandy tsunami and storm deposits using modern examples. Sediment. Geol. 200 (3–4), 184–207.

Morton, R.A., Goff, J.R., Nichol, S.L., 2008. Hydrodynamic implications of textural trends in sand deposits of the 2004 tsunami in Sri Lanka. Sediment. Geol. 207 (1–4), 56–64.

Muravyev, Y.D., Fedotov, S.A., Budnikov, V.A., Ozerov, A.Y., Magus'kin, M.A., Dvigalo, V.N., Andreyev, V.I., Ivanov, V.V., Kartasheva, L.A., Markov, I.A., 1998. Volcanic activity in the Karymsky center in 1996: summit eruption at Karymsky and phreatomagmatic eruption in the Akademii Nauk caldera. Volcanology and Seismology 19, 567–604.

Narayana, A.C., Tatavarti, R., Shinu, N., Subeer, A., 2007. Tsunami of December 26, 2004 on the southwest coast of India: post-tsunami geomorphic and sediment characteristics. Mar. Geol. 242, 155–168.

Paris, R., 2015. Source mechanisms of volcanic tsunamis. Phil. Trans. R. Soc. A 373, 20140380.

Paris, R., Wassmer, P., Lavigne, F., Belousov, A., Belousova, M., Iskandarsyah, Y., Benbakkar, M., Ontowirjo, B., Mazzoni, N., 2014. Coupling eruption and tsunami records: the Krakatau 1883 case-study, Indonesia. Bull. Volcanol. 76, 814.

Pilarczyk, J.E., Horton, B.P., Witter, R.C., Vane, C.H., Chagué-Goff, C., Goff, J., 2012. Sedimentary and foraminiferal evidence of the 2011 Tohoku-oki tsunami on the Sendai coastal plain, Japan. Sediment. Geol. 282, 78–89.

Srinivasalu, S., Thangadurai, N., Jonathan, M.P., Armstrong-Altrin, J.S., Ayyamperumal, T., Ram Mohan, V., 2008. Evaluation of trace-metal enrichments from the 26 December 2004 tsunami sediments along the Southeast coast of India. Environ. Geol. 53, 1711–1721.

Switzer, A., Pucillo, K., Haredy, R., Jones, B., Bryant, E., 2005. Sea level, storm, or tsunami: enigmatic sand sheet deposits in a sheltered coastal embayment from southeastern New South Wales, Australia. J. Coast. Res. 21, 655–663.

Switzer, A., Srinivasalu, S., Thangadurai, N., Mohan, W.R., 2012. Bedding structures in Indian tsunami deposits that provide clues to the dynamics of tsunami inundation. Geol. Soc. Lond., Spec. Publ. 361, 61–77.

Szczuciński, W., Chaimanee, N., Niedzielski, P., Rachlewicz, G., Saisuttichai, D., Tepsuwan, T., Lorenc, S., Siepak, J., 2006. Environmental and geological impacts of the 26 December 2004 tsunami in coastal zone of Thailand — overview of short and long-term effects. Pol. J. Environ. Stud. 15 (5), 793–810.

Szczuciński, W., Kokociński, M., Rzeszewski, M., Chagué-Goff, C., Cachao, M., Goto, K., Sugawara, D., 2012. Sediment sources and sedimentation processes of 2011 Tohoku-oki tsunami deposits on the Sendai Plain, Japan — insights from diatoms, nannoliths and grain size distribution. Sediment. Geol. 282, 40–56.

Torsvik, T., Paris, R., Didenkulova, I., Pelinovsky, E., Belousov, A., Belousova, M., 2010. Numerical simulation of explosive tsunami wave generation and propagation in Karymskoye Lake, Russia. Nat. Hazards Earth Syst. Sci. 10 (11), 2359–2369.

Ulvrová, M., Paris, R., Kelfoun, K., Nomikou, P., 2014. Numerical simulations of tsunami generated by underwater volcanic explosions at Karymskoye Lake (Kamchatka, Russia) and Kolumbo volcano (Aegean Sea, Greece). Nat. Hazards Earth Syst. Sci. 14, 401–412.

Wohletz, K.H., 1986. Explosive magma-water interactions: thermodynamics, explosion mechanisms, and field studies. Bull. Volcanol. 48, 245–2654.